THE JOURNAL OF PHYSICAL CHEMISTRY C
A JOURNAL OF THE AMERICAN CHEMICAL SOCIETY

pubs.acs.org/JPCC
Article

Electromagnetically Induced Absorption Overcomes the Upper Limit of Light Absorption: Dipole−Dipole Coupling with Phase Retardation in Plasmonic-Dielectric Dimers

Kishin Matsumori,* Ryushi Fujimura, and Markus Retsch

Cite This: J. Phys. Chem. C 2023, 127, 19127−19140
Read Online

ACCESS | Metrics & More | Article Recommendations | Supporting Information

ABSTRACT: Electromagnetically induced absorption (EIA) by a phase-retarded coupling is theoretically investigated using a dimer composed of a plasmonic and dielectric particle. This phase-retarded coupling originates from the particles interacting with each other through their scattered intermediate fields (in between near and far fields). Our analysis based on the coupled-dipole method and an extended coupled-oscillator model indicates that EIA by the phase-retarded coupling occurs due to constructive interference in the scattered fields of the particles. By employing the finite element method, we demonstrate that the absorption of the plasmonic particle is dramatically enhanced by tuning the interparticle distance and achieving constructive interference. In contrast to EIA by near-field coupling, which has been intensively researched using coupled plasmonic systems, EIA by a phase-retarded coupling enables us to strengthen the absorption of plasmonic systems more significantly. This significant absorption enhancement is expected to be beneficial to advancing various applications, such as energy harvesting and radiative cooling.

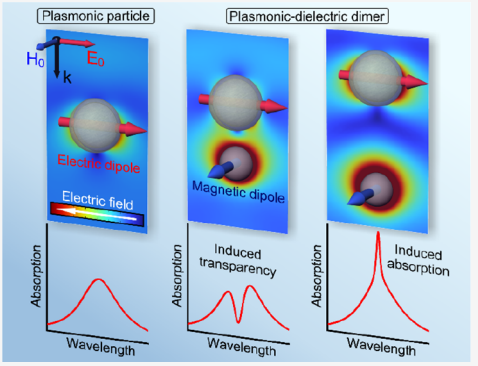

1. INTRODUCTION

Light absorption is of fundamental importance for various applications. The field of plasmonics has attracted considerable attention since localized surface plasmons (LSPs) can confine electromagnetic fields beyond the optical diffraction limit and enhance light absorption. Strong light absorption is induced at the resonance of the LSPs, which can be controlled by designing the composition, shape, and size of a plasmonic structure. Given the high tunability of the LSPs, plasmonic structures have been designed in different wavelength ranges to advance emerging applications such as energy harvesting,[1] solar-thermophotovoltaics,[2,3] radiative cooling,[4] sensing,[5−7] IR camouflage,[8] and optical heating.[9−11] To enhance light absorption of materials, different absorption mechanisms have been utilized, such as impedance matching,[12−15] Kerker effect,[16−18] and rainbow trapping.[19−21]

In addition to those optical phenomena, electromagnetically induced absorption (EIA) can be a potential approach to strengthening the absorption of plasmonic systems. EIA was first observed in atomic systems as a substantial absorption enhancement of the system by constructive quantum interference.[22,23] In contrast, destructive quantum interference results in electromagnetically induced transparency (EIT), which creates a transparency window in absorption spectra.[24] Since interference phenomena in quantum and classical systems are analogous, EIA-like effects have been realized in plasmonic systems. One of the most commonly used plasmonic systems for EIA is a coupled system composed of a bright and dark oscillators.[25−29] The bright oscillator possesses a high total (ohmic + radiative) damping and can be excited by the external incident wave. On the other hand, the dark oscillator exhibits low total damping and is excited only by coupling to the electromagnetic near field of the bright oscillator. EIA has been extensively investigated and applied to perfect light absorbers,[30] optical modulators,[31,32] and nonlinear effects.[33] However, mechanistic interpretations of EIA have contained ambiguity so far.

In our previous work, we developed the unified interpretation of EIA by investigating the absorption properties of coupled plasmonic systems known for EIA: plasmonic-polymer composite and dipolar-quadrupolar antennas.[34] We concluded that their EIA is attributed to the absorption enhancement of the dark oscillator by near-field coupling, enabling the total absorption of the entire system to possess an EIA-like spectral profile (see Figure 1a). However, the absorption of the bright oscillator always has an EIT-like profile, meaning that the near-field coupling process is equivalent to destructive interference

Received: May 18, 2023
Revised: August 10, 2023
Published: September 15, 2023

https://doi.org/10.1021/acs.jpcc.3c03307
J. Phys. Chem. C 2023, 127, 19127−19140

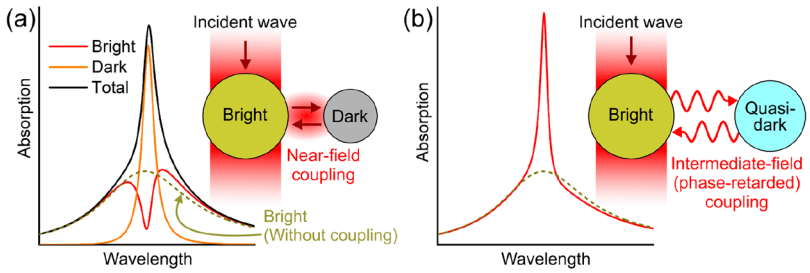

Figure 1. Schematic illustrations of plasmonic EIA excited by (a) near-field coupling and (b) phase-retarded coupling.

and contradicts EIA observed in the atomic systems. Moreover, we found that EIA of the plasmonic systems can enhance the dark oscillator's absorption up to 1/4 of the maximum extinction of the isolated bright oscillator (without coupling to the dark oscillator). This finding indicates that the total absorption of the entire system cannot exceed the upper absorption bound of the isolated bright oscillator, which is given by $C_{abs} = 3\lambda_0^2/8\pi$ for a dipolar antenna (C_{abs} is the absorption cross-section, and λ_0 is the resonance wavelength).[35−38]

Mimicking EIA of the atomic systems in plasmonic systems and searching for means to overcome $C_{abs} = 3\lambda_0^2/8\pi$ by constructive interference are of great interest not only for the applications mentioned earlier but also for the physics of plasmonics.[39−43] One of the approaches to achieving constructive interference in plasmonic systems may be utilizing a phase-retarded coupling. The phase-retarded coupling has been investigated by using, for example, waveguides[44,45] and dimers made of two scattering particles.[46−53] In the case of the dimers, interactions between particles can be characterized by two dipole moments, and the phase-retarded coupling occurs by far-field interactions. It has been observed that scattering and absorption of the dimers are strengthened and weakened by controlling their interparticle distance, which may correspond to constructive and destructive interference, respectively.[50−52] However, a rigorous understanding of the phase-retarded coupling has not been given. Also, EIA-like effects have not yet been confirmed in the dimers.

In this work, we theoretically investigate EIA excited by the phase-retarded coupling using a dimer consisting of a plasmonic and dielectric particles. An LSP of the plasmonic particle and a Mie resonance of the dielectric particle exhibit dipolar resonances with high and low damping, respectively. Considering this damping contrast and that both dipolar resonances can be excited directly by the incident wave, the plasmonic and dielectric particles are characterized as bright and quasi-dark oscillators, respectively (Figure 1b). To interpret the phase-retarded coupling of this plasmonic-dielectric system, we first discuss the scattering properties of isolated plasmonic and dielectric particles by considering their dipole moments. Next, we investigate dipole−dipole coupling of the dimer using the coupled-dipole method (CDM). Based on the CDM, we design an extended coupled-oscillator (ECO) model to give an intuitive picture of the coupling. The ECO model suggests that three forces are working on each particle with different phases, and those phases can be controlled by changing the interparticle distance of the dimer. Consequently, the interparticle distance determines whether the coupling in the dimer becomes constructive or destructive, resulting in EIA or EIT, respectively. These effects of the phase-retarded coupling on the absorption properties of the dimer are demonstrated by performing the finite element method (FEM) simulation. With an optimal interparticle distance of the dimer, we show that EIA by the phase-retarded coupling enhances the absorption of the plasmonic particle beyond $C_{abs} = 3\lambda_0^2/8\pi$ at a resonance condition (Figure 1b). To the best of our knowledge, this type of EIA has been observed only in the interactions between an LSP and waveguide mode.[34,54]

2. THEORY AND METHODS

2.1. Scattered Fields of Electric and Magnetic Dipole Moments. Plasmonic and dielectric particles with subwavelength scales can be approximated as a dipolar antenna. The optical properties of the dipolar antenna are described by its electric dipole (ED) moment $\mathbf{p}_j$ and magnetic dipole (MD) moment $\mathbf{m}_j$. The ED and MD moments at $\mathbf{r}_j$ in free space are[55]

$$\mathbf{p}_j = \varepsilon_0 \alpha_j \mathbf{E}_{in}(\mathbf{r}_j) \tag{1}$$

$$\mathbf{m}_j = \chi_j \mathbf{H}_{in}(\mathbf{r}_j) \tag{2}$$

where ε_0 is the electric permittivity in a vacuum, α_j is the electric polarizability, and χ_j is the magnetic polarizability. $\mathbf{E}_{in}(\mathbf{r}_j) = \mathbf{E}_0 e^{i\mathbf{k}\cdot\mathbf{r}_j}$ and $\mathbf{H}_{in}(\mathbf{r}_j) = \mathbf{H}_0 e^{i\mathbf{k}\cdot\mathbf{r}_j}$ are the incident electric and magnetic fields, respectively. $\mathbf{k}$ is the wave vector ($|\mathbf{k}| = 2\pi/\lambda$, where λ is the wavelength of the incident field). Scattered electric and magnetic fields at $\mathbf{r}_i$ created by the ED moment are expressed as

$$\mathbf{E}_{spj}(\mathbf{r}_i) = \frac{1}{\varepsilon_0}\mathbf{G}_E(\mathbf{r}_i - \mathbf{r}_j)\cdot\mathbf{p}_j \tag{3}$$

$$\mathbf{H}_{spj}(\mathbf{r}_i) = \frac{1}{\varepsilon_0 Z_0}\mathbf{G}_M(\mathbf{r}_i - \mathbf{r}_j)\cdot\mathbf{p}_j \tag{4}$$

Similarly, scattered fields of the MD moment are

$$\mathbf{E}_{smj}(\mathbf{r}_i) = -Z_0\mathbf{G}_M(\mathbf{r}_i - \mathbf{r}_j)\cdot\mathbf{m}_j \tag{5}$$

$$\mathbf{H}_{smj}(\mathbf{r}_i) = \mathbf{G}_E(\mathbf{r}_i - \mathbf{r}_j)\cdot\mathbf{m}_j \tag{6}$$

where Z_0 is the vacuum impedance. $\mathbf{G}_E$ and $\mathbf{G}_M$ are the dyadic Green's functions, which are expressed using $\mathbf{r}_i - \mathbf{r}_j = D\mathbf{u}_r$ (D and $\mathbf{u}_r$ are the distance and unit vector of $\mathbf{r}_i - \mathbf{r}_j$, respectively):

$$\mathbf{G}_E(\mathbf{r}_i - \mathbf{r}_j)\cdot\mathbf{u} = g_A\mathbf{u} + g_B(\mathbf{u}_r\cdot\mathbf{u})\mathbf{u}_r \tag{7}$$

$$\mathbf{G}_M(\mathbf{r}_i - \mathbf{r}_j)\cdot\mathbf{u} = g_C(\mathbf{u}_r \times \mathbf{u}) \tag{8}$$

where $\mathbf{u}$ is the arbitrary unit vector. Equations 7 and 8 have the relationship of $\mathbf{G}_E(\mathbf{r}_i - \mathbf{r}_j) = \mathbf{G}_E(\mathbf{r}_j - \mathbf{r}_i)$ and $\mathbf{G}_M(\mathbf{r}_i - \mathbf{r}_j) = -\mathbf{G}_M(\mathbf{r}_j - \mathbf{r}_i)$, respectively. The terms g_A, g_B, and g_C in eqs 7 and 8 are

https://doi.org/10.1021/acs.jpcc.3c03307
J. Phys. Chem. C 2023, 127, 19127−19140

$$g_A = \frac{e^{ikD}}{4\pi D}\left(k^2 + \frac{ik}{D} - \frac{1}{D^2}\right) \quad (9)$$

$$g_B = \frac{e^{ikD}}{4\pi D}\left(-k^2 - \frac{3ik}{D} + \frac{3}{D^2}\right) \quad (10)$$

$$g_C = \frac{e^{ikD}}{4\pi D}\left(k^2 + \frac{ik}{D}\right) \quad (11)$$

Equations 9−11 describe the amplitude and phase of the scattered fields. The scattered field of dipole moments can be categorized into three regions by comparing D with λ: the near (static) field for $D \ll \lambda$, the intermediate (induction) field for $D \approx \lambda$, and the far (radiation) field for $D \gg \lambda$ (see Figure 2a).

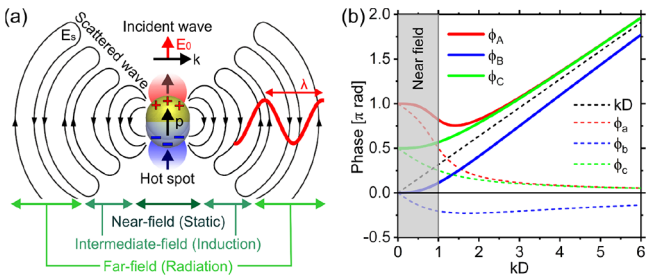

Figure 2. (a) Schematic illustration of a scattered electric field created by a plasmonic particle. The scattered field can be categorized into three fields: the near field ($D << \lambda$), intermediate field ($D \approx \lambda$), and far field ($D >> \lambda$). There is no clear boundary between those fields, and the illustration just gives an intuitive picture of those boundaries. (b) Phases given by eqs 15−17. Those are plotted as a function of kD. The red, blue, and green solid lines are the net phases of ϕ_A, ϕ_B, and ϕ_C, respectively. The red, blue, and green dashed lines are ϕ_a, ϕ_b, and ϕ_c, respectively. The gray shaded area indicates the near field determined by $kD < 1$. Since $kD = 2\pi D/\lambda \approx 6D/\lambda$ and the intermediate field is $D \approx \lambda$, the plot is in a range of the near and intermediate fields.

Considering Maxwell's equations and the wave equation, each field has a time derivation in different orders: 0-th, 1-th, and 2nd order derivation for the static, induction, and radiation fields, respectively. We consider the time-harmonic system; therefore, by setting the static field as a reference, the induction and radiation fields are $\pi/2$, and π phase shifted, respectively. Equations 9−11 can be modified as

$$g_A = \frac{1}{4\pi D}\sqrt{\left(k^2 - \frac{1}{D^2}\right)^2 + \left(\frac{k}{D}\right)^2}\, e^{i[kD + \arg(k^2 + \frac{ik}{D} - \frac{1}{D^2})]} = |g_A| e^{i\phi_A} \quad (12)$$

$$g_B = \frac{1}{4\pi D}\sqrt{\left(-k^2 + \frac{3}{D^2}\right)^2 + \left(\frac{3k}{D}\right)^2}\, e^{i[kD + \arg(-k^2 - \frac{3ik}{D} + \frac{3}{D^2})]} = |g_B| e^{i\phi_B} \quad (13)$$

$$g_C = \frac{1}{4\pi D}\sqrt{k^4 + \left(\frac{k}{D}\right)^2}\, e^{i[kD + \arg(k^2 + \frac{ik}{D})]} = |g_C| e^{i\phi_C} \quad (14)$$

where $|g_A|$, $|g_B|$, and $|g_C|$ are the scattered field amplitude, and arg() is the argument of a complex function. Note that the CDM cannot express the near-field property since the scattered field amplitudes diverge with $D \to 0$. The net phases denoted as ϕ_A, ϕ_B, and ϕ_C can be divided into two terms

$$\phi_A = kD + \arg\left(k^2 + \frac{ik}{D} - \frac{1}{D^2}\right) = kD + \phi_a \quad (15)$$

$$\phi_B = kD + \arg\left(-k^2 - \frac{3ik}{D} + \frac{3}{D^2}\right) = kD + \phi_b \quad (16)$$

$$\phi_C = kD + \arg\left(k^2 + \frac{ik}{D}\right) = kD + \phi_c \quad (17)$$

In eqs 15−17, kD can be considered a background phase. ϕ_a, ϕ_b, and ϕ_c express influences from the near and intermediate fields. Equations 15−17 are shown in Figure 2b. The contributions from the near and intermediate fields are substantial at a small D. This contribution decreases and becomes negligible for a large D; therefore, the net phases are dominated by kD in the far field. From eqs 15−17, we can understand that the scattered fields have different phases depending on the direction and distance from the dipole moments.

We consider two dipole moments interacting with each other in the different fields defined in Figure 2a. For a near-field interaction occurring through the hot spots, the interaction is expected to occur instantaneously with the oscillations of the dipole moments. This type of interaction has been extensively researched since an electromagnetic field can be strongly confined between the dipoles.[56−61] When the distance between the dipole moments is in a region of $D > \lambda$, a far-field interaction has to be considered. In that far-field case, each dipole moment is oscillated by the scattered field of another dipole moment with phase delay determined by eqs 15−17. This phase-retarded coupling may provide additional control for light-matter interactions and allow for achieving EIA. In the far field, the phase can be controlled in a wide range by tuning D. However, eqs 12−14 indicate that the scattered field amplitudes are weakened with an increase in D. Since a strong interaction requires a strong electromagnetic field, it is challenging to achieve a strong interaction in the far field. However, the intermediate field can possess moderately strong field amplitude and phase control simultaneously. By considering these advantages of the intermediate field, we will outline how the phase-retarded coupling results in EIA.

2.2. Phase-Retarded Coupling. The phase-retarted coupling is investigated by considering that a plasmonic particle interacts with a dielectric particle, and they are oriented along the propagation direction of the incident wave. In general, any particles possess ED and MD moments; therefore, a four-dipole (FD) model has to be used for a complete analysis of the optical properties of a dimer (Figure 3a). However, a plasmonic particle has a strong ED moment by a localized surface plasmon (LSP) and its MD moment is negligibly weak.[60] A dielectric particle possesses both ED and MD moments by Mie resonances. ED and MD of a dielectric particle with a low refractive index usually spectrally overlap with each other. With a high refractive index, a dielectric particle can resolve its ED and MD. Therefore, a dimer composed of plasmonic and high-index dielectric particles allows us to reduce the FD model to two-dipole (TD) models (see Figure 3b).

Using the TD models and CDM,[59,60,62,63] we observe how excitation states of the LSP and Mie resonances change by the intermediate-field coupling. The incident wave propagates along the z-direction with $\mathbf{E}_{in}(\mathbf{r}_j) = E_0\hat{\mathbf{e}}_x e^{i\mathbf{k}\cdot\mathbf{r}_j}$ and $\mathbf{H}_{in}(\mathbf{r}_j) = H_0\hat{\mathbf{e}}_y e^{i\mathbf{k}\cdot\mathbf{r}_j}$, where $\hat{\mathbf{e}}$ is the unit vector in the Cartesian

https://doi.org/10.1021/acs.jpcc.3c03307
J. Phys. Chem. C 2023, 127, 19127−19140

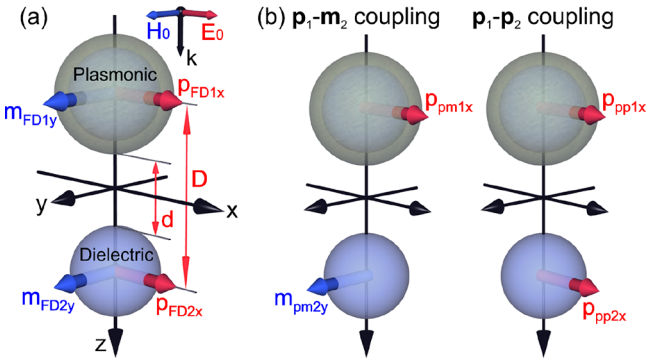

Figure 3. Schematic illustrations of the dimer composed of plasmonic and dielectric particles. (a) The FD model considers all dipole moments of the dimer. (b) The TD models involve only two dipole moments.

coordinate system. The plasmonic and dielectric particles locate at $\mathbf{r}_1 = (0, 0, -D/2)$ and $\mathbf{r}_2 = (0, 0, D/2)$, respectively. Under this condition, we first consider a $\mathbf{p}_1$-$\mathbf{m}_2$ coupling of the dimer based on our previous work.[64] The ED moment of the plasmonic particle $\mathbf{p}_{pm1}$ and the MD moment of the dielectric particle $\mathbf{m}_{pm2}$ are given using eqs 1−6 as

$$\begin{aligned}\mathbf{p}_{pm1} &= \varepsilon_0\alpha_1[\mathbf{E}_{in}(\mathbf{r}_1) + \mathbf{E}_{sm2}(\mathbf{r}_1)] \\ &= \varepsilon_0\alpha_1[E_0\hat{\mathbf{e}}_x e^{-i(kD/2)} - Z_0\mathbf{G}_M(\mathbf{r}_1 - \mathbf{r}_2)\cdot\mathbf{m}_{pm2}]\end{aligned} \tag{18}$$

$$\begin{aligned}\mathbf{m}_{pm2} &= \chi_2[\mathbf{H}_{in}(\mathbf{r}_2) + \mathbf{H}_{sp1}(\mathbf{r}_2)] \\ &= \chi_2\left[H_0\hat{\mathbf{e}}_y e^{i(kD/2)} + \frac{1}{\varepsilon_0 Z_0}\mathbf{G}_M(\mathbf{r}_2 - \mathbf{r}_1)\cdot\mathbf{p}_{pm1}\right]\end{aligned} \tag{19}$$

For spherical particles, the electric and magnetic polarizabilities can be given as $\alpha = (6\pi i/k^3)a_1$ and $\chi = (6\pi i/k^3)b_1$, where a_1 and b_1 are Mie coefficients for first-order electric and magnetic modes, respectively.[62,65] These polarizabilities may be approximated using the Lorentz oscillator[37]

$$\alpha_j = \frac{f_{pj}}{\omega_{pj}^2 - \omega^2 - i\Gamma_{pj}\omega} = \frac{f_{pj}}{\Omega_{pj}} \tag{20}$$

$$\chi_j = \frac{f_{mj}}{\omega_{mj}^2 - \omega^2 - i\Gamma_{mj}\omega} = \frac{f_{mj}}{\Omega_{mj}} \tag{21}$$

where f_{pj} and f_{mj} are the oscillator strength, ω_{pj} and ω_{mj} are the angular resonance frequencies, and Γ_{pj} and Γ_{mj} are the damping rates. ω is the angular frequency in free space. Using eqs 18−21, self-consistent forms of $\mathbf{p}_{pm1}$ and $\mathbf{m}_{pm2}$ are (S1, Supporting Information)

$$\mathbf{p}_{pm1} = p_{pm1x}\hat{\mathbf{e}}_x = \frac{\Omega_{p1}\Omega_{m2} - \Omega_{p1}f_{m2}|g_C|e^{i(\phi_C + kD)}}{\Omega_{p1}\Omega_{m2} + f_{p1}f_{m2}|g_C|^2 e^{i2\phi_C}}\mathbf{p}_1 \tag{22}$$

$$\mathbf{m}_{pm2} = m_{pm2y}\hat{\mathbf{e}}_y = \frac{\Omega_{p1}\Omega_{m2} + \Omega_{m2}f_{p1}|g_C|e^{i(\phi_C - kD)}}{\Omega_{p1}\Omega_{m2} + f_{p1}f_{m2}|g_C|^2 e^{i2\phi_C}}\mathbf{m}_2 \tag{23}$$

where $\mathbf{p}_1$ and $\mathbf{m}_2$ are the ED moment of the isolated plasmonic particle and the MD moment of the isolated dielectric particle, respectively (see eqs 1 and 2). Equations 22 and 23 show that the dipole moments of the dimer result from the dipole moments of the isolated particles modulated by interactions through their scattered field. In a similar manner to the $\mathbf{p}_1$-$\mathbf{m}_2$ coupling, we investigate a $\mathbf{p}_1$-$\mathbf{p}_2$ coupling by considering that the dielectric particle only has an ED at the resonance of the LSP of the plasmonic particle. In this case, the ED moments of the plasmonic particle $\mathbf{p}_{pp1}$ and the dielectric particle $\mathbf{p}_{pp2}$ are expressed as (S1, Supporting Information)

$$\mathbf{p}_{pp1} = p_{pp1x}\hat{\mathbf{e}}_x = \frac{\Omega_{p1}\Omega_{p2} + \Omega_{p1}f_{p2}|g_A|e^{i(\phi_A + kD)}}{\Omega_{p1}\Omega_{p2} - f_{p1}f_{p2}|g_A|^2 e^{i2\phi_A}}\mathbf{p}_1 \tag{24}$$

$$\mathbf{p}_{pp2} = p_{pp2x}\hat{\mathbf{e}}_x = \frac{\Omega_{p1}\Omega_{p2} + \Omega_{p2}f_{p1}|g_A|e^{i(\phi_A - kD)}}{\Omega_{p1}\Omega_{p2} - f_{p1}f_{p2}|g_A|^2 e^{i2\phi_A}}\mathbf{p}_2 \tag{25}$$

In eqs 22−25, we can find that those interacting dipole moments contain the phase terms originating from the scattered fields. These results suggest that the dipole moments can be controlled by distance-dependent phase retardation, and the amplitude of the dipole moments can be enhanced if the dipole moments can couple constructively.

We provide an intuitive understanding of the phase-retarded coupling by designing an ECO model. Our ECO model shown in Figure 4a comprises two mechanical harmonic oscillators:

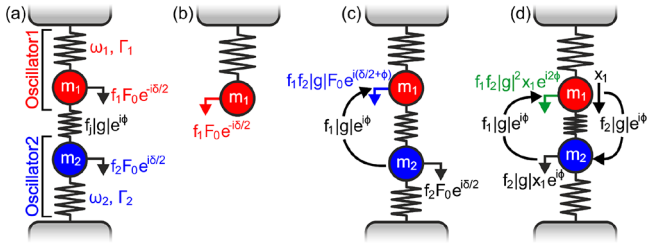

Figure 4. (a) Schematic illustration of the ECO model. (b−d) Schematic illustrations of (b) the first, (c) second, and (d) third terms of eq 30.

Oscillator1 and Oscillator2 correspond to the plasmonic and dielectric particles in Figure 3, respectively. The equations of motion of the ECO model are given as

$$\frac{d^2x_1}{dt^2} + \Gamma_1\frac{dx_1}{dt} + \omega_1^2 x_1 - f_1|g|e^{i\phi}x_2 = f_1F_0(t)e^{-i\delta/2} \tag{26}$$

$$\frac{d^2x_2}{dt^2} + \Gamma_2\frac{dx_2}{dt} + \omega_2^2 x_2 - f_2|g|e^{i\phi}x_1 = f_2F_0(t)e^{i\delta/2} \tag{27}$$

where x_j is the displacement of the mass objects, ω_j is the angular resonant frequency, and Γ_j is the damping rate. Oscillator1 has a higher damping rate than Oscillator2, meaning $\Gamma_1 > \Gamma_2$. In our previous work, we demonstrated that the damping of plasmonic systems needs to be distinguished into intrinsic and radiative damping to fully characterize their optical properties.[34] However, in this work, we are interested in phenomenological analysis to understand the oscillation state of the plasmonic-dielectric dimer. Therefore, for simplicity, we only consider the total damping (intrinsic + radiative) of the particles. $f_jF_0(t)$ is the external force working on the oscillators. The external force is time-harmonic; therefore, $F_0(t) = F_0e^{-i\omega t}$ where F_0 is the amplitude of the external force. f_j describes the coupling rate of the

https://doi.org/10.1021/acs.jpcc.3c03307
J. Phys. Chem. C 2023, 127, 19127−19140

oscillator to the external force and corresponds to the oscillator strength of the polarizabilities (see eqs 20 and 21). f_j is normalized by the mass of the oscillator m_j. The external force includes the phase term determined by δ to consider that the LSP of the plasmonic particle and the Mie resonance of the dielectric particle are oscillated with different phases by the incident wave. This is because the dimer axis of Figure 3 is parallel to the propagation direction of the incident field. Next, we consider the coupling between Oscillator1 and Oscillator2. From the CDM, we know that the LSP of the plasmonic particle couples with the Mie resonance of the dielectric particle through their scattered fields. In the ECO model, the scattered field amplitude is represented as $|g|$. Each oscillator couples to the scattered field of another oscillator with the coupling rate of f_j. Therefore, the coupling strength of each oscillator is given by $f_j|g|$. As explained earlier, the scattered field involves the phase delay ϕ, resulting in a phase-retarded coupling of $f_j|g|e^{i\phi}$. A modification of eqs 26 and 27 gives

$$x_1 = \frac{1}{\Omega_1}\left[f_1 F_0(t)e^{-i\delta/2} + f_1|g|e^{i\phi}x_2\right] \tag{28}$$

$$x_2 = \frac{1}{\Omega_2}\left[f_2 F_0(t)e^{i\delta/2} + f_2|g|e^{i\phi}x_1\right] \tag{29}$$

where $\Omega_j = \omega_j^2 - \omega^2 - i\Gamma_j\omega$. In eq 28, the first term is the direct influence of the external force on Oscillator1 (see Figure 4b). The second term means that the oscillation of Oscillator2 works on Oscillator1 through the phase-retarded coupling. The same interpretation can be applied to eq 29. Substituting eq 29 into eq 28 gives

$$x_1 = \frac{1}{\Omega_1}\left\{f_1 F_0(t)e^{-i\delta/2} + \frac{1}{\Omega_2}\left[f_1 f_2|g|F_0(t)e^{i(\phi+(\delta/2))} + f_1 f_2|g|^2 e^{i2\phi}x_1\right]\right\} \tag{30}$$

The second term of eq 30 describes the effect of the external force $f_2F_0(t)e^{i\delta/2}$ working on Oscillator1 (see Figure 4c). The third term shows a round-trip coupling process of $x_1 \rightarrow x_2 \rightarrow x_1$ (see Figure 4d), which is described in two steps: (A) the oscillation of Oscillator1 works on Oscillator2 through the coupling of $f_2|g|e^{i\phi}$. (B) This coupling oscillates Oscillator2, and the oscillation of Oscillator2 works back on Oscillator1 through the coupling of $f_1|g|e^{i\phi}$. Therefore, the round-trip coupling involves a total phase delay of 2ϕ.[50] A self-consistent form of eq 30 is

$$x_1 = \frac{\Omega_1\Omega_2 + \Omega_1 f_2|g|e^{i(\phi+\delta)}}{\Omega_1\Omega_2 - f_1 f_2|g|^2 e^{i2\phi}}\left[\frac{f_1}{\Omega_1}F_0(t)e^{-i\delta/2}\right] \tag{31}$$

Equation 31 coincides with $\mathbf{p}_{pp1}$ given by eq 24. The $\mathbf{p}_1$-$\mathbf{m}_2$ coupling can also be described by the same coupling processes shown in Figure 4. Considering the coupling processes described in Figure 4, it can be found that three forces work on Oscillator1, and those forces have different phases. Therefore, if those phases allow the forces to work on Oscillator1 constructively, the displacement amplitude of Oscillator1 can be enhanced. From the CDM, the phase of the coupling is a function of the interparticle distance D, meaning that the coupling may occur constructively by controlling D. By comparing the ECO model and the CDM, we can find that the coupling strength in the CDM is expressed by a combination of the oscillator strength of the polarizabilities (f_{pj} and f_{mj}), and the scattered field amplitudes ($|g_A|$ and $|g_C|$). As can be seen in eqs 12 and 14, the scattered field amplitudes dramatically decrease with an increase in D even in the intermediate field. Therefore, f_{pj} and f_{mj} must be sufficiently large to achieve strong coupling between distant particles.

2.3. Constructive and Destructive Interference in the Dimer. We figure out a condition of EIA originating from the phase-retarded coupling. As explained in the introduction, there are two types of EIA: EIA induced by near-field or phase-retarded coupling. EIA by a near-field coupling is dominated by the absorption enhancement in the dark oscillator. In contrast, for EIA by a phase-retarded coupling, it is expected that an absorption enhancement occurs in the bright oscillator since the oscillation of the bright oscillator can be amplified by the coupling (see eq 31). In the plasmonic-dielectric dimer, the plasmonic particle corresponds to the bright oscillator. Therefore, the dimer may possess an EIA-like spectral profile even though the dielectric particle, which corresponds to the quasi-dark oscillator, has no absorption. Based on this, to simplify our investigation, we consider that the dielectric particle is lossless (no intrinsic damping), and the plasmonic particle solely determines the absorption properties of the dimer. The optical properties of the plasmonic particle are dominated by the ED of the LSP. For the dimer, extinction, scattering, and absorption cross-sections of the ED are given as (S2, Supporting Information)[63]

$$C_{\mathrm{extED}j} = \frac{k}{\varepsilon_0|\mathbf{E}_0|^2}\mathrm{Im}[\mathbf{p}_{nj}\cdot\mathbf{E}_{\mathrm{in}}^*(\mathbf{r}_j)] \tag{32}$$

$$C_{\mathrm{scaED}j} = \frac{k}{\varepsilon_0|\mathbf{E}_0|^2}\mathrm{Im}\left[\left(\frac{ik^3}{6\pi\varepsilon_0} + \frac{1}{\varepsilon_0\alpha_j}\right)|\mathbf{p}_{nj}|^2 - \mathbf{p}_{nj}^*\cdot\mathbf{E}_{\mathrm{in}}(\mathbf{r}_j)\right] \tag{33}$$

$$C_{\mathrm{absED}j} = C_{\mathrm{extED}j} - C_{\mathrm{scaED}j} = \frac{k}{\varepsilon_0|\mathbf{E}_0|^2}\mathrm{Im}\left[-\left(\frac{ik^3}{6\pi\varepsilon_0} + \frac{1}{\varepsilon_0\alpha_j}\right)\right]|\mathbf{p}_{nj}|^2 \tag{34}$$

The subscript n represents n ∈ (pm, pp). In eqs 32−34, an isotropic electric polarizability is considered. From eq 34, the absorption of the plasmonic particle is proportional to the absolute square of its ED moment. When the resonances of the particles of the dimer are aligned, meaning that $\omega_{p1} = \omega_{m2}$ for the $\mathbf{p}_1$-$\mathbf{m}_2$ coupling and $\omega_{p1} = \omega_{p2}$ for the $\mathbf{p}_1$-$\mathbf{p}_2$ coupling, $|\mathbf{p}_{n1}|^2$ is given as ($\omega_{p1} = \omega_{m2} = \omega_{p2} = \omega_0$) (S3, Supporting Information)

$$|\mathbf{p}_{pm1}|^2 = \frac{1 + \Phi_{pm2}^2 + 2\Phi_{pm2}\sin(\phi_C + kD)}{1 + \Phi_{pm}^2 + 2\Phi_{pm}\cos(2\phi_C + \pi)}|\mathbf{p}_1|^2 = P_{pm}|\mathbf{p}_1|^2 \tag{35}$$

$$|\mathbf{p}_{pp1}|^2 = \frac{1 + \Phi_{pp2}^2 + 2\Phi_{pp2}\sin(-\phi_A - kD)}{1 + \Phi_{pp}^2 + 2\Phi_{pp}\cos(2\phi_A)}|\mathbf{p}_1|^2 = P_{pp}|\mathbf{p}_1|^2 \tag{36}$$

where

https://doi.org/10.1021/acs.jpcc.3c03307
J. Phys. Chem. C 2023, 127, 19127−19140

$$\Phi_{pm} = \frac{f_{p1}f_{m2}\,|g_C|^2}{\Gamma_{p1}\Gamma_{m2}\omega_0^2} = \frac{f_{p1}|g_C|}{\Gamma_{p1}\omega_0}\frac{f_{m2}|g_C|}{\Gamma_{m2}\omega_0} = \Phi_{pm1}\Phi_{pm2} \quad (37)$$

$$\Phi_{pp} = \frac{f_{p1}f_{p2}\,|g_A|^2}{\Gamma_{p1}\Gamma_{p2}\omega_0^2} = \frac{f_{p1}|g_A|}{\Gamma_{p1}\omega_0}\frac{f_{p2}|g_A|}{\Gamma_{p2}\omega_0} = \Phi_{pp1}\Phi_{pp2} \quad (38)$$

Φ_n is the ratio of the coupling strength to the total damping of the dimer. This ratio describes how strongly the particles couple with each other.[34] Φ_{nj} is the ratio of the coupling strength to the damping of each particle. When there is no coupling ($\Phi_{nj} = 0$), eqs 35 and 36 coincide with $|\mathbf{p}_1|^2$. The sine and cosine functions of eqs 35 and 36 describe the influence of phase retardation in the coupling. Depending on those functions, it is determined whether $|\mathbf{p}_{n1}|^2$ can be amplified. Therefore, we can understand that the function P_n (in eqs 35 and 36) describes the phase-retarded coupling, and EIA is induced when $P_n > 1$.

For a fundamental understanding of P_n, we employ a systematic analysis using a simplified form of P_n

$$P = \frac{1 + \Phi_2^2 + 2\Phi_2 \sin\theta_S}{1 + \Phi^2 + 2\Phi\cos\theta_C},\ \Phi = \Phi_1\Phi_2 \quad (39)$$

where θ_S and θ_C are the angles for the sine and cosine functions, respectively. Φ and Φ_j are dimensionless and unitless values. P is the most amplified when $\sin\theta_S = 1$ and $\cos\theta_C = -1$ occur simultaneously. This is a condition for EIA excited by complete constructive interference. We first consider how Φ_1 and Φ_2 influence P under complete constructive interference. In Figure 5a, we can find that P is

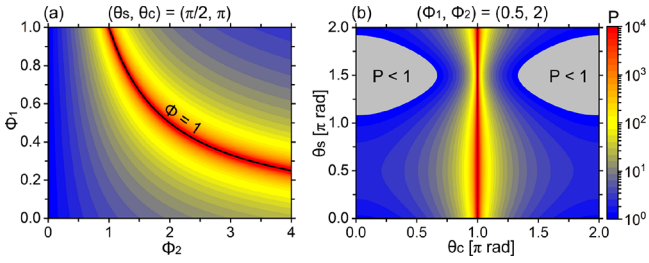

Figure 5. (a) Color map of eq 39 as functions of Φ_1 and Φ_2. $(\theta_S, \theta_C) = (\pi/2, \pi)$ is used. (b) Color map of eq 39 as functions of θ_C and θ_S. $(\Phi_1, \Phi_2) = (0.5, 2)$ is used.

significantly enhanced at $\Phi = 1$. This is because P diverges at $\Phi = 1$. Considering eqs 37 and 38, $\Phi = 1$ means that the damping of the entire system takes balance with the energy transferred between two dipole moments. This situation can be recognized as a critical coupling.[34] When a set of (Φ_1, Φ_2) makes $\Phi \neq 1$, P decreases no matter which is larger Φ_1 or Φ_2. Next, we investigate the influences of (θ_S, θ_C) on P. Figure 5b shows P as functions of θ_S and θ_C. $(\Phi_1, \Phi_2) = (0.5, 2)$ is used for this color map. As expected from eq 39, P increases for $(\theta_S, \theta_C) \rightarrow (\pi/2, \pi)$ and decreases for $(\theta_S, \theta_C) \rightarrow (3\pi/2, 0 \text{ or } 2\pi)$. It is found that $P > 1$ can be obtained even though complete constructive interference is not achieved. Therefore, partially constructive interference ($(\theta_S, \theta_C) \neq (\pi/2, \pi)$ but $P > 1$) can also contribute to EIA. The gray shaded areas of Figure 5b indicate $P < 1$, meaning that the coupling is destructive and EIA cannot be observed. The same properties of P shown in Figure 5b can be applied to P with different (Φ_1, Φ_2). However, if Φ becomes larger or smaller than 1, the area of $P < 1$ increases, and the overall intensity of P decreases (S4, Supporting Information).

Our systematic analysis using P suggests that $\Phi = 1$ and complete constructive interference must occur simultaneously to maximize EIA. However, Hugonin et al. indicated that the upper bounds of absorption of any dimers may be determined independently of their material properties.[52] Therefore, this extreme condition may not be achieved since Φ is connected to material properties. Our analysis also suggests that the condition for EIA is not confined to the extreme condition and demonstrates that EIA may be induced under partially constructive interference.

Since satisfying the extreme condition is not straightforward, we focus on partially constructive interference in this work. From eqs 37 and 38, (Φ_1, Φ_2) is determined by the polarizabilities of the particles and the scattered field amplitude. (θ_S, θ_C) is solely determined by the phase of the scattered fields. If the design and materials of the particles are determined, the polarizabilities are immediately given. In this case, P can be expressed as a function only of D. Therefore, we may be able to find an optimal D for EIA just by calculating P and finding its maximum.

2.4. Design and Optical Properties of the Particles.

Plasmonic and dielectric particles of the dimer are designed to theoretically demonstrate EIA as discussed earlier. We use a concentric core-shell geometry for the plasmonic particle (see Figure 6a). The plasmonic core-shell particle consists of a dielectric core with radius r_{CS} being fully covered with a plasmonic shell with a thickness of t_{CS}. The core-shell structure has been widely used in plasmonics, and it is known that its LSP can be controlled by tuning the aspect ratio of the outer to inner radii. In addition, its scattering and absorption properties can also be controlled by changing the aspect ratio.[35,38,39,66] For a dielectric particle, a sphere with a radius of r_S is used. Compared to the LSP, a Mie resonance of a dielectric sphere is relatively easily controlled by tuning r_S since the Mie resonance is not confined by the Fröhlich condition.[67]

Next, proper materials for the plasmonic core-shell particle and the dielectric sphere have to be chosen. We first consider the material for the dielectric sphere. To realize the $\mathbf{p}_1$-$\mathbf{m}_2$ and $\mathbf{p}_1$-$\mathbf{p}_2$ coupling, a refractive index of the dielectric sphere has to be sufficiently large to spectrally separate its ED and MD resonances. Silicon, which has been intensively used for nanophotonics,[68] possesses a high refractive index of about 3.5,[69] but the ED and MD resonances are close to each other with a refractive index of this value. A refractive index higher than that of silicon can be accessible from infrared (IR) dielectric materials, such as PbTe and Bi_2Te_3.[70,71] Based on those considerations, a complex refractive index of the dielectric sphere $N_S = n_S + i\kappa_S$ has to be determined. We chose $n_S = 5.6$ by referring to the refractive index of PbTe. As mentioned earlier, we simplify the system by considering a lossless dielectric sphere, meaning $\kappa_S = 0$; therefore, $N_S = n_S$ (later, we will consider the case of $\kappa_S \neq 0$). Since the material we consider for the dielectric sphere is for the IR region, materials of the plasmonic core-shell particle also have to be for that wavelength range. Metal oxides, such as AZO, are representative plasmonic materials in the IR region.[69] Therefore, we use an AZO shell for the plasmonic core-shell particle. We assume that the dielectric core has a constant refractive index of $N_{CS} = 1.55$, which can be obtained by polymers, such as polystyrene .[72]

https://doi.org/10.1021/acs.jpcc.3c03307
J. Phys. Chem. C 2023, 127, 19127−19140

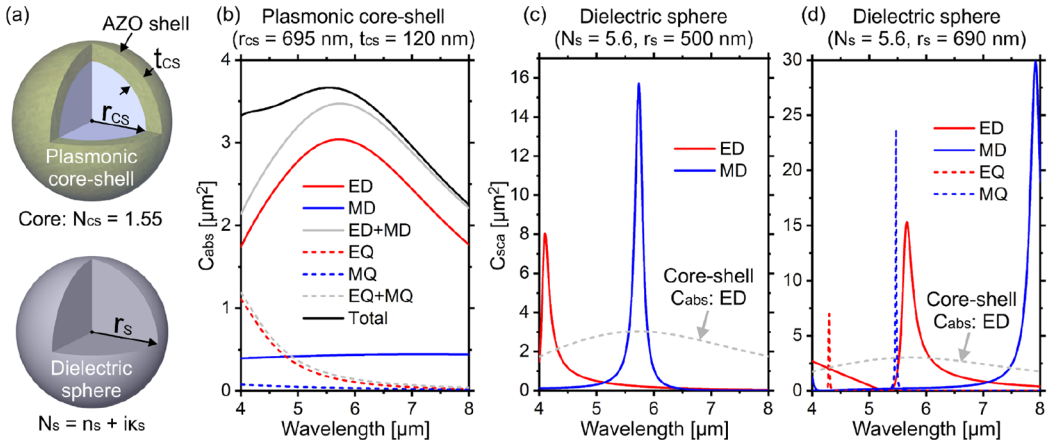

Figure 6. Optical properties of the plasmonic and dielectric particles. (a) Schematic illustrations of the plasmonic core-shell particle and dielectric sphere. The core-shell particle is composed of the AZO shell and dielectric inner core with a refractive index of N_{CS} = 1.55. The shell thickness and inner core radius are t_{CS} and r_{CS}, respectively. The dielectric sphere with the radius of r_S has the complex refractive index of $N_S = n_S + i\kappa_S$. (b) Absorption properties of the plasmonic core-shell particle. The red, blue, and gray solid lines are for the ED, MD, and total absorption of the dipolar resonances, respectively. The red, blue, and gray dashed lines are for the EQ, MQ, and total absorption of the quadrupolar resonances, respectively. (c, d) Scattering properties of the dielectric spheres with r_S = 500 and 690 nm. The red and blue solid lines are for the ED and MD, respectively. The red and blue dashed lines are for the EQ and MQ, respectively. The gray dashed line is the absorption spectrum of the ED of the plasmonic core-shell particle, which is taken from panel b.

The absorption properties of the isolated plasmonic core-shell particle are shown in Figure 6b. The absorption of the ED, MD, electric quadrupole (EQ), and magnetic quadruple (MQ) are calculated using Mie theory.[65] The refractive index of AZO is taken from ref 69. r_{CS} and t_{CS} are determined so that the ED absorption is roughly maximized by satisfying $C_{abs} \approx C_{sca}$ (S5, Supporting Information).[36] This is because we are interested in observing that EIA enhances the absorption of the plasmonic core-shell particle beyond the upper absorption limit of an isolated particle $C_{abs} = 3\lambda_0^2/8\pi$. The absorption of the plasmonic core-shell particle is dominated by the ED. The MD has a nearly constant absorption over the wavelength range. The EQ and MQ contribute to the total absorption at short wavelengths.

Scattering cross-section (C_{sca}) spectra of the dielectric spheres with different radii are shown in Figure 6c,d. As mentioned earlier, since the dielectric spheres are lossless, they do not possess any absorption. For both spheres, ED and MD resonances are well resolved. The dielectric spheres with r_S = 500 and 690 nm have the MD and ED at the absorption peak of the plasmonic core-shell particle, respectively. Therefore, the $\mathbf{p}_1$-$\mathbf{m}_2$ and $\mathbf{p}_1$-$\mathbf{p}_2$ coupling can be investigated using the plasmonic core-shell particle and those dielectric spheres. The dielectric sphere with r_S = 690 nm possesses a strong MQ resonance right next to the ED resonance. This MQ resonance may disturb observing the $\mathbf{p}_1$-$\mathbf{p}_2$ coupling.

Note that our discussion made here is based on Mie theory, which provides multipole resonances of a spherical particle by multipolar decomposition on a spherical basis. In addition to this spherical multipolar decomposition, Cartesian multipolar decomposition (CMD) has been widely recognized.[73−76] In CMD, the ED resonance of Mie theory is further decomposed to an ED resonance on a Cartesian basis (ED_{car}) and a toroidal dipole resonance. The scattered field created by the ED_{car} and toroidal dipole resonances can interfere with each other in the far-field and create an anapole state when a certain condition is satisfied.[77−80] For our particles, their toroidal dipole resonances are weak, and we cannot see any anapoles (Figure S2b, Supporting Information). Therefore, we can safely ignore the influence of the toroidal dipole resonances.

2.5. Numerical Calculations. In the following section, the optical properties of the dimer will be discussed in detail. C_{abs} and C_{sca} of the dimer were obtained using COMSOL Multiphysics, which is a commercial software package based on the FEM. The orientations of the dimer and the incident plane wave are shown in Figure 3a. The plasmonic core-shell particle and dielectric sphere designed in Figure 6 were used. The surrounding of the dimer was air, and a perfectly matched layer (PML) was applied around the calculation domain. C_{abs} was calculated by taking the volume integral of energy dissipation density over the dimer. C_{sca} was calculated by taking the surface integral of the Poynting vector of the scattered field over the integration sphere, which was defined between the dimer and PML.

The optical cross-sections of the dimer were also calculated using the CDM. So far, we have only discussed interactions between two dipole moments. This can be valid for phenomenological analysis. However, as seen in Figure 6b−d, there are small contributions from other dipole moments of the plasmonic core-shell particle and dielectric sphere (for example, the MD of the plasmonic core-shell particle), which must be considered for a complete analysis. Therefore, we calculated the optical properties of the dimer by using the FD model shown in Figure 3a (S1 and S2, Supporting Information). In these calculations, the polarizabilities were not approximated by the Lorentz functions, but those were given by Mie coefficients for accurate analysis. For simplicity, our CDM calculations do not consider quadrupole moments,[81] but the plasmonic core-shell particle has an EQ and MQ in a short wavelength range. Therefore, the contributions from the quadrupole moments were taken into account in the total absorption of the dimer by adding EQ + MQ of the plasmonic core-shell particle, which is given by Mie theory (Figure S4, Supporting Information).

https://doi.org/10.1021/acs.jpcc.3c03307
J. Phys. Chem. C 2023, 127, 19127−19140

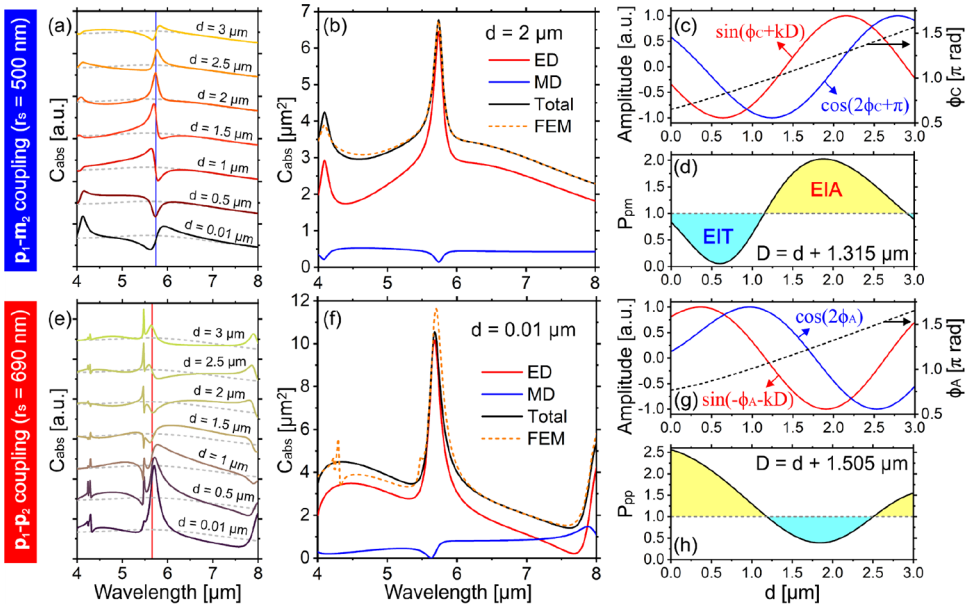

Figure 7. (Top row) $\mathbf{p}_1$-$\mathbf{m}_2$ coupling of the dimer composed of the dielectric sphere with r_S = 500 nm. (Bottom row) $\mathbf{p}_1$-$\mathbf{p}_2$ coupling of the dimer composed of the dielectric sphere with r_S = 690 nm. (a, e) d dependencies of the absorption of the dimer. The absorption spectra are calculated using the FEM simulation. The gray dashed lines are the reference spectra given by the total absorption of the isolated plasmonic core-shell particle (Figure 6b). The blue and red solid vertical lines show the resonance wavelengths of the MD and ED of the dielectric spheres, respectively. (b, f) The solid lines are the absorption spectra of the dimer, which are calculated using the CDM. The red and blue solid lines are for the ED and MD of the plasmonic core-shell particle. The black solid line is the total absorption of the plasmonic core-shell particle (Figure S4, Supporting Information). The orange dashed lines are taken from Figure 7a,e. (c, g) The sine and cosine functions of P_{pm} (eq 35) and P_{pp} (eq 36) are plotted as a function of d on the left vertical axis. The phases of ϕ_C and ϕ_A are shown as the black dashed lines on the right vertical axis. (d, h) P_{pm} and P_{pp} are calculated at $\omega_0 = \omega_{m2} = 3.29 \times 10^{14}$ rad/s and $\omega_0 = \omega_{p2} = 3.33 \times 10^{14}$ rad/s, respectively.

3. RESULTS AND DISCUSSION

The absorption properties of the dimer are presented in Figure 7. We first focus on the $\mathbf{p}_1$-$\mathbf{m}_2$ coupling shown in the top row of Figure 7. The dielectric sphere with r_S = 500 nm is used in the dimer. Figure 7a shows absorption spectra of the dimer with different face-to-face distances d (Figure 3a), which are obtained using the FEM simulation. Since the dielectric sphere is lossless, the absorption properties of the dimer are dominated by the plasmonic core-shell particle. The gray dashed lines are the reference spectra given by the total absorption of the isolated plasmonic core-shell particle (from Figure 6b). When d is small, the absorption spectra have an absorption dip around the MD resonance of the dielectric sphere (the blue vertical line of Figure 7a). This spectral profile can be recognized as EIT. In contrast, the absorption is strongly enhanced with increasing d, and a sharp absorption peak appears at the MD resonance of the dielectric sphere when d is around 2 μm. This absorption enhancement is attributed to EIA. With a further increase in d, the absorption spectra again show the EIT-like spectral profile.

In Figure 7b, the absorption of the dimer with d = 2 μm is calculated using the CDM. The black solid line is the total absorption of the plasmonic core-shell particle. The orange dashed line is the absorption taken from Figure 7a. Comparing the black solid and orange dashed lines, we find that the CDM is in good agreement with the FEM simulation, which proves that the CDM is a proper method to investigate the absorption properties of the dimer. This agreement can be confirmed for different d and the scattering properties of the dimer (S6, Supporting Information). The red and blue solid lines are the ED and MD absorptions of the plasmonic core-shell particle, respectively. It can be found that the ED absorption possesses a pronounced peak over a broad absorption, characterizing EIA by the phase retarded coupling. Interestingly, this absorption enhancement enables the plasmonic core-shell particle to exceed the upper absorption limit of $C_{abs} = 3\lambda_0^2/8\pi \approx 3.9\ \mu m^2$ at $\lambda_0 \approx 5.7\ \mu$m, which cannot be achieved by EIA induced by near-field coupling.[34]

We investigate the EIA of the dimer using P_{pm} (eq 35). P_{pm} contains $\sin(\phi_C + kD)$ and $\cos(2\phi_C + \pi)$, which are functions of D. D is the center-to-center distance of the dimer; therefore, $D = d + (r_{CS} + t_{CS}) + r_S$. Figure 7c shows $\sin(\phi_C + kD)$ and $\cos(2\phi_C + \pi)$ as a function of d. It can be found that complete constructive interference cannot be achieved by the $\mathbf{p}_1$-$\mathbf{m}_2$ coupling. To better understand the EIA of the dimer, P_{pm} has to be calculated using the variables of the polarizabilities. The variables can be extracted by fitting the Lorentz functions to the polarizabilities given by Mie coefficients (S5, Supporting Information). The fitting results are summarized in Table 1. In Figure 7d, P_{pm} with $\omega_0 = \omega_{m2}$ is plotted using these extracted values and the sine and cosine functions in Figure 7c.

Table 1. Oscillator Strengths, Resonance Frequencies, and Damping Rates of the Polarizabilities[a]

Lorentz oscillator	core-shell particle electric polarizability	sphere (r_S = 500 nm) magnetic polarizability	sphere (r_S = 690 nm) electric polarizability
f_j [m^3·(rad/s)^2]	4.35×10^{11}	4.3×10^{10}	7.83×10^{10}
ω_j [rad/s]	3.31×10^{14}	3.29×10^{14}	3.33×10^{14}
Γ_j [rad/s]	2.38×10^{14}	9.11×10^{12}	1.72×10^{13}

[a]These values are obtained by fitting the Lorentz oscillator (eqs 20 and 21) to the polarizabilities given by Mie coefficients. The details can be found in S5, Supporting Information.

https://doi.org/10.1021/acs.jpcc.3c03307
J. Phys. Chem. C 2023, 127, 19127−19140

Depending on d, P_{pm} can be smaller or larger than 1. When $P_{pm} < 1$ (blue shaded area of Figure 7d), the absorption of the plasmonic core-shell particle is decreased by destructive interference, resulting in the EIT-like spectral profile. In contrast, $P_{pm} > 1$ (yellow shaded area of Figure 7d) means that constructive interference enhances the absorption of the plasmonic core-shell particle, enabling us to observe the EIA-like spectral profile. P_{pm} is maximized at around $d = 2$ μm, which can be the optimum d for EIA. These results from P_{pm} coincide with the FEM simulation shown in Figure 7a, proving that P_{pm} is an applicable function for investigating the EIA of the dimer. At $d = 2$ μm, the scattered field amplitude is $|g_C| = 2.98 \times 10^{16}$ m^{-3}, which gives $(\Phi_{pm1}, \Phi_{pm2}, \Phi_{pm}) = (0.17, 0.43, 0.07)$. Φ_{pm} is much smaller than 1, suggesting that the critical coupling cannot be achieved in this $\mathbf{p}_1$-$\mathbf{m}_2$ coupling.

We turn our focus to the $\mathbf{p}_1$-$\mathbf{p}_2$ coupling shown in the bottom row of Figure 7. In this case, the dielectric sphere with $r_S = 690$ nm is used. Figure 7e shows d dependency of the absorption of the dimer. There are sharp absorption dips and peaks at around the wavelengths of 4.2 and 5.5 μm, which are attributed to the influence of the EQ and MQ of the dielectric sphere, respectively (see Figure 6d). At around the ED resonance of the dielectric sphere (the red vertical line of Figure 7e), we can see that the absorption spectra change from EIA → EIT → EIA-like profile with an increase in d. The dimer system with $d = 0.01$ μm has the strongest absorption, which is examined using the CDM in Figure 7f. The CDM (black solid line) and the FEM simulation (orange dashed line) are in good agreement, but the discrepancy between them is slightly larger than that for the $\mathbf{p}_1$-$\mathbf{m}_2$ coupling. This is because our CDM calculations do not take the influence of the EQ and MQ of the dielectric sphere into account. Furthermore, the discrepancy originates from the fact that the CDM cannot fully describe the near-field effect. $d = 0.01$ μm means that the particles of the dimer are nearly touching each other. In this situation, the near-field effect may be expected to dominate the $\mathbf{p}_1$-$\mathbf{p}_2$ coupling. However, considering the orientations of the dimer and the incident wave, the electromagnetic hot spots of the particles weakly influence the $\mathbf{p}_1$-$\mathbf{p}_2$ coupling. This is because the hot spots are concentrated in the x-direction so that the ED moments of the particles do not directly interact through the hot spots. Therefore, there is a near-field effect in the $\mathbf{p}_1$-$\mathbf{p}_2$ coupling, but the intermediate-field effect dominates the $\mathbf{p}_1$-$\mathbf{p}_2$ coupling. Figure 7f shows that the ED absorption of the plasmonic core-shell particle is strongly enhanced by the $\mathbf{p}_1$-$\mathbf{p}_2$ coupling. Compared to the case of the $\mathbf{p}_1$-$\mathbf{m}_2$ coupling, the absorption enhancement for the $\mathbf{p}_1$-$\mathbf{p}_2$ coupling is more significant.

To understand this absorption enhancement, we use P_{pp} (eq 36). Figure 7g shows $\sin(-\phi_A - kD)$ and $\cos(2\phi_A)$ of P_{pp}, indicating that complete constructive interference cannot be achieved by the $\mathbf{p}_1$-$\mathbf{p}_2$ coupling. Using Figure 7g and the extracted electric polarizability of the dielectric sphere (see Table 1), P_{pp} is calculated at $\omega_0 = \omega_{p2}$ and plotted in Figure 7h. P_{pp} suggests that the $\mathbf{p}_1$-$\mathbf{p}_2$ coupling becomes constructive → destructive → constructive with an increase in d, which coincide with the spectral change shown in Figure 7e. From the agreement between the results in Figure 7e,h, we can find that the optimum d for EIA is 0.01 μm. $d = 0.01$ μm gives the scattered field amplitude $|g_A| = 5.69 \times 10^{16}$ m^{-3}. Using this value, we get $(\Phi_{pp1}, \Phi_{pp2}, \Phi_{pp}) = (0.31, 0.77, 0.24)$. This Φ_{pp} is larger than $\Phi_{pm} = 0.07$, resulting in stronger EIA for the $\mathbf{p}_1$-$\mathbf{p}_2$ coupling than for the $\mathbf{p}_1$-$\mathbf{m}_2$ coupling. In addition to the absorption properties of the dimer, one can find the scattering properties of the dimer with the $\mathbf{p}_1$-$\mathbf{m}_2$ and $\mathbf{p}_1$-$\mathbf{p}_2$ couplings (Figures S6 and S7, Supporting Information).

For experiments and applications related to sunlight, such as solar absorbers, we must understand whether EIA presented here can be excited under an unpolarized incident wave. To induce EIA, our theory suggests that constructive interference of the following three waves must occur at the position of the plasmonic particle: the incident wave, the scattered wave of the dielectric particle, and the round-trip scattered wave (see Figure 4). This constructive interference can be achieved only when their electric fields are oriented in the same direction. However, under an unpolarized incident wave, the directions of their electric fields may be different. Thus, the waves cannot interfere or can only weakly interfere. Having understood this, we conclude that EIA may not be induced under an unpolarized incident wave even though the dimer is symmetric from the view of the incident wave's propagation.

Here, we briefly summarize the finding from Figure 7. The dimer involves the phase-retarded coupling, and its EIA is attributed to partially constructive interference. An optimum d for EIA can be found relatively easily by calculating P_{pm} and P_{pp} for the $\mathbf{p}_1$-$\mathbf{m}_2$ and $\mathbf{p}_1$-$\mathbf{p}_2$ coupling, respectively. It must be mentioned that the dimer possesses different absorption properties if the positions of the plasmonic core-shell particle and dielectric sphere are swapped. By doing this, an EIA-like spectral profile cannot be observed in the absorption of the dimer (S7, Supporting Information). We have only discussed the absorption properties of the dimer oriented parallel to the propagation direction of the incident wave. In S8 and S9 of Supporting Information, we investigate the absorption properties of the dimer oriented perpendicular to the propagation direction of the incident wave. Our investigation reveals that EIA can be excited in the dimer with different orientations. Furthermore, we also investigate the n_S dependency of the absorption properties of the dimer (S10, Supporting Information). Even though n_S is smaller than 5.6, EIA can be observed. Since P_{pm} and P_{pp} increase and decrease depending on their sine and cosine functions, one might expect that there is a characteristic kD maximizing EIA. If this is true, an optimal D is immediately found when the resonance condition of the dimer is determined. However, P_{pm} and P_{pp} also depend on the material properties of the dimer (eqs 37 and 38). Thus, an optimal kD for EIA changes when a different dimer is investigated (S11, Supporting Information).

For an insight into constructive and destructive interference of the dimer, we observe electric field distribution maps obtained using the FEM simulation. Figure 8a is a reference electric field map of the isolated plasmonic core-shell particle at its ED resonance ($\lambda_0 = 5.72$ μm). Figure 8b shows the $\mathbf{p}_1$-$\mathbf{m}_2$ coupling of the dimer. From Figure 7d, it is known that the absorption of the plasmonic core-shell particle in the dimer with $d = 0.5$ and 2 μm possesses the EIT-like and EIA-like spectral profiles, respectively. The field maps of Figure 8b are taken at around the absorption dip ($\lambda_0 = 5.73$ μm) for $d = 0.5$ μm and the absorption peak ($\lambda_0 = 5.74$ μm) for $d = 2$ μm. The electric field around the plasmonic core-shell particle is much stronger for $d = 2$ μm than for $d = 0.5$ μm. In general, it might be expected that the electric field enhancement is stronger for the dimer with a smaller d because the electric fields of each particle are strong at a point close to the particles, and strong coupling can occur if the particles are close to each other. However, as explained earlier, the coupling involves phase

https://doi.org/10.1021/acs.jpcc.3c03307
J. Phys. Chem. C 2023, 127, 19127−19140

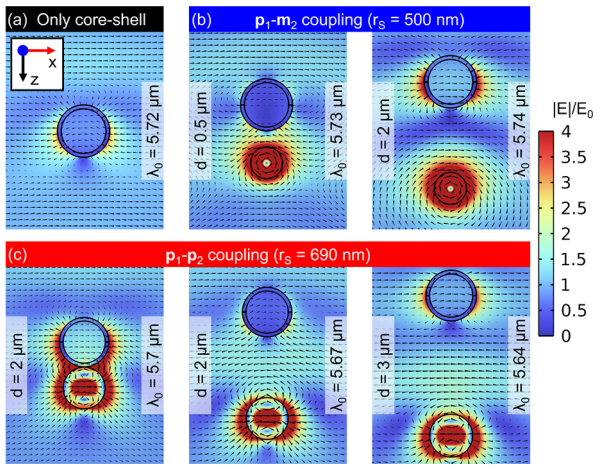

Figure 8. Electric field distribution maps. The absolute values of the electric fields are normalized by the electric field amplitude of the incident wave. The black arrows are electric field vectors. (a) The field map for the isolated plasmonic core-shell particle at its ED resonance. (b) The field maps of the dimer with r_S = 500 nm. d = 0.5 and 2 μm are chosen to observe the destructive and constructive coupling, respectively. (c) The field maps of the dimer with r_S = 690 nm. d = 0.01, 2, and 3 μm are used to show the transition of constructive → destructive → constructive interference. Additional field analyses can be found in S12, Supporting Information.

retardation, which can make the coupling destructive or constructive depending on d. Therefore, the electric field of the plasmonic core-shell particle can be strengthened even though d is large. This field enhancement occurs through the scattered intermediate field without relying on the electric field hot spots. In Figure 8c, the field maps for the $\mathbf{p}_1$-$\mathbf{p}_2$ coupling are presented. The dimers with d = 0.01, 2, and 3 μm are considered for those field maps. Those interparticle distances are chosen based on the findings in Figure 7e,h: with increasing d, the absorption of the plasmonic core-shell particle changes EIA → EIT → EIA-like profile. Therefore, the electric field around the plasmonic core-shell particle is weak for d = 2 μm (at λ_0 = 5.67 μm), and it becomes strong for d = 0.01 μm (at λ_0 = 5.7 μm) and d = 3 μm (at λ_0 = 5.64 μm). The dimer with d = 0.01 μm possesses the strongest electric field of the plasmonic core-shell particle because constructive interference occurs with a small d, meaning that the coupling is significantly strong.

Additional electric field analyses can be found in S12, Supporting Information. From previous studies, it has been known that the absorption spectrum of a plasmonic system blueshifts from its near-field spectrum.[82−85] This spectral shift of the optical responses can also be seen for EIA (Figure S18, Supporting Information). By analyzing the near field of the plasmonic particle of the dimer, one can find unique dispersion properties of EIA by the phase retarded coupling, which may provide a better understanding of the destructive and constructive couplings (Figures S19 and S20, Supporting Information).

We have considered a dimer with a lossless dielectric sphere. However, real dielectric materials are usually not lossless. Here, we investigate the influences of an intrinsic loss κ_S of the dielectric sphere on the EIA properties of the dimer. For this investigation, the $\mathbf{p}_1$-$\mathbf{m}_2$ coupling is considered, and the dimer with r_S = 500 nm and d = 2 μm is used. Figure 9a shows how the absorption properties of an isolated dielectric sphere with r_S = 500 nm and n_S = 5.6 change with an increase in κ_S. Those spectra are calculated using Mie theory. The absorption becomes pronounced with increasing κ_S up to about 0.1. With

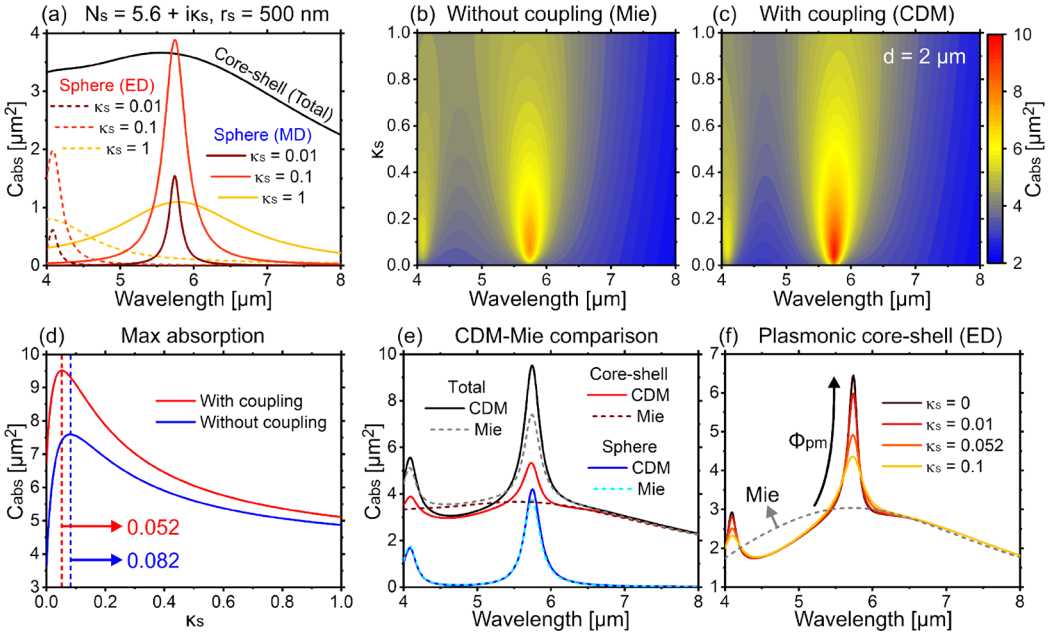

Figure 9. κ_S dependency. (a) Absorption properties of the isolated dielectric sphere with N_S = 5.6 + $i\kappa_S$ and r_S = 500 nm. The solid and dashed lines are for the MD and ED, respectively. The black solid line is the total absorption of the plasmonic core-shell particle, taken from Figure 6b. (b, c) Color maps of the total absorption of the dimer with r_S = 500 nm and d = 2 μm, which are calculated using Mie theory and CDM for without and with coupling, respectively. (d) Maximum absorptions of Figure 9b,c.Those are plotted as a function of κ_S. (e) Absorption properties of the plasmonic core-shell particle and dielectric sphere with κ_S = 0.052 in the dimer with d = 2 μm. The solid and dashed lines are calculated using the CDM and Mie theory, respectively. (f) Influence of κ_S on the ED absorption of the plasmonic core-shell particle.

https://doi.org/10.1021/acs.jpcc.3c03307
J. Phys. Chem. C 2023, 127, 19127−19140

a further increase in κ_S, the absorption decreases and becomes broad.

Suppose there is no coupling effect in the dimer. In this case, the total absorption of the dimer is given by a superposition of the absorptions of the isolated plasmonic core-shell particle and isolated dielectric sphere. The dielectric sphere with a moderately high κ_S possesses a strong absorption. Therefore, the total absorption of the dimer with the lossy dielectric sphere can be strong even though EIA does not exist. In other words, the total absorption of the dimer can be improved further if EIA of the plasmonic core-shell particle coincides with the strong absorption of the dielectric sphere. To figure out whether the phase-retarded coupling can positively affect the absorption properties of the dimer with $\kappa_S \neq 0$, the total absorption spectra of the dimer without and with coupling are plotted in Figure 9b,c as functions of κ_S and λ. The absorption of the dimer without coupling is given by the sum of the absorptions of the isolated plasmonic core-shell particle and isolated dielectric sphere in Figure 9a. The absorption of the dimer with coupling is calculated using the CDM. Comparing Figure 9c to Figure 9b, the absorption properties for with-coupling are similar to those for without coupling. A strong absorption peak is found around the MD resonance of the dielectric sphere. This pronounced peak is broadened with an increase in κ_S.

In Figure 9d, the maxima of the absorption spectra in Figure 9b,c are plotted as a function of κ_S. The maximum absorption for with coupling is larger than without coupling for any κ_S. The peak of the maximum absorption for with coupling appears at $\kappa_S \approx 0.052$. Figure 9e shows the absorption spectra of the dimer with $\kappa_S = 0.052$. Those spectra are calculated using Mie theory and the CDM for without and with coupling, respectively. The absorption spectra of the plasmonic core-shell particle and dielectric sphere are separately obtained by taking their ED + MD (the EQ + MQ is considered only for the plasmonic core-shell particle). The results from the CDM are in good agreement with the FEM simulation even though the lossy dielectric sphere is considered (Figure S21, Supporting Information). For with coupling (the CDM), the absorption spectral profile of the plasmonic core-shell particle is similar to what we observed in Figure 7b, which is the case of $\kappa_S = 0$. This result indicates that the EIA properties of the plasmonic core-shell particle discussed earlier are preserved even though $\kappa_S \neq 0$. The absorption of the dielectric sphere is slightly enhanced by the coupling. But its spectral shape is almost the same as the spectrum from Mie theory, meaning that the absorption properties of the dielectric sphere are not significantly influenced by the phase-retarded coupling (S7, Supporting Information). From the results in Figure 9e, it is understood that the dimer with coupling can possess EIA of the plasmonic core-shell particle and the strong absorption of the dielectric sphere simultaneously. When the plasmonic core-shell particle does not couple with the dielectric sphere, EIA obviously has no contribution to the total absorption of the dimer. Thus, the phase-retarded coupling can have a positive effect on improving the total absorption of the dimers with any κ_S.

Comparing with and without coupling in Figure 9d, their peaks are located at different κ_S. The peak for without coupling appears at $\kappa_S = 0.082$. When there is no coupling effect between the plasmonic core-shell particle and dielectric sphere, the maximum absorption of the dimer is determined by the absorption of the dielectric sphere. The absorption of an isolated particle is maximized when $C_{abs} \approx C_{sca}$ is satisfied. For the dielectric sphere with $n_S = 5.6$ and $r_S = 500$ nm, this condition is satisfied with $\kappa_S \approx 0.082$ (Figure S22, Supporting Information). Therefore, the peak for without coupling appears at $\kappa_S \approx 0.082$. However, as mentioned earlier, the peak for with coupling is found at $\kappa_S = 0.052$. When the plasmonic core-shell particle couples with the dielectric sphere, the maximum absorption of the dimer is determined not only by the absorption of the dielectric sphere but also by EIA of the plasmonic core-shell particle. From Figure 7, it is known that EIA occurs on the ED resonance of the plasmonic core-shell particle. Figure 9f shows how the ED absorption of the plasmonic core-shell particle changes depending on κ_S. Those spectra are calculated using the CDM, and the dimer with $d = 2$ μm is considered. With an increase in κ_S, EIA becomes weak, which can be described using Φ_{pm}. For the dimer investigated in Figure 9, f_{p1}, Γ_{p1}, ω_0, and $|g_C|$ are constant. f_{m2} is also nearly constant for different κ_S, but only Γ_{m2} increases with increasing κ_S because κ_S directly connects to the intrinsic damping of the dielectric sphere (S13, Supporting Information). Therefore, Φ_{pm} decreases with increasing κ_S, resulting in weak coupling. In consequence, EIA of the plasmonic core-shell particle attenuates. Based on understanding how EIA is weakened by κ_S, we can find why the peaks for with and without coupling in Figure 9d appear at different κ_S. The absorption of the dielectric sphere increases with increasing κ_S up to 0.082; however, the EIA of the plasmonic core-shell particle keeps decreasing with increasing κ_S. Therefore, the peak for with coupling locates at κ_S slightly lower than that for without coupling.

In summary, constructive interference can occur between the plasmonic core-shell particle and the dielectric sphere even though the dielectric sphere contains $\kappa_S \neq 0$. This constructive interference can enhance the total absorption of the dimer with any κ_S. As seen in Figure 9d, κ_S is an essential parameter to maximize the total absorption of the dimer. Since κ_S is determined by material properties, controlling κ_S is not straightforward. But if it is possible to control κ_S, an optimal κ_S may be found at around κ_S satisfying $C_{abs} \approx C_{sca}$ for the isolated dielectric sphere. However, an increase in κ_S weakens the coupling effect because κ_S increases the damping of the entire system, resulting in weak EIA. Therefore, if it is required to maximize the absorption of the plasmonic core-shell particle, the dielectric sphere must be lossless.

4. CONCLUSIONS

We investigated the mechanism of EIA induced by a phase-retarded coupling between plasmonic and dielectric particles. We formulated the phase-retarded coupling using the CDM, enabling us to find the optimum interparticle distances of the dimer to achieve EIA (P_{pm}: eq 35, P_{pp}: eq 36). This formulation suggested that EIA can be strengthened by balancing the coupling strength and the total damping of the dimer (Φ_{pm}: eq 37, Φ_{pp}: eq 38). We obtained the absorption spectra of the dimer using the FEM simulation and CDM, showing that the absorption of the plasmonic particle is significantly enhanced when the interparticle distance of the dimer is optimized. This result demonstrated that EIA by the phase-retarded coupling strengthens the bright oscillator's absorption, which is different from EIA by the near-field coupling in coupled plasmonic systems.[34] Our numerical analysis suggested that EIA by the phase-retarded coupling allows the plasmonic particle to overcome the upper

https://doi.org/10.1021/acs.jpcc.3c03307
J. Phys. Chem. C 2023, 127, 19127−19140

absorption bound of an isolated particle. In contrast, EIA excited by the near-field coupling cannot achieve this significant absorption enhancement.[34] EIA properties of the dimer can be preserved even though the dielectric particle is made of lossy material; however, EIA becomes weak with an increase in the dielectric particle's extinction coefficient. In this work, we only presented a dimer composed of two spherical particles. Our interpretation of EIA can be applied to many systems consisting of two dipolar optical elements, providing a route to engineer the optical properties of heterostructured materials.

■ ASSOCIATED CONTENT

Supporting Information

The Supporting Information is available free of charge at https://pubs.acs.org/doi/10.1021/acs.jpcc.3c03307.

Details of the coupled-dipole method, calculations of optical cross-sections, optical properties of the isolated particles, scattering properties of the dimer, absorption properties of the dimer with different orientations, systematic analyses of P functions, near-field analyses, and n_S and κ_S dependencies of the absorption properties of the dimer (PDF)

■ AUTHOR INFORMATION

Corresponding Author

Kishin Matsumori − *Department of Chemistry, Physical Chemistry I, University of Bayreuth, Bayreuth 95447, Germany;* orcid.org/0000-0002-5615-9032; Email: kishin.matsumori@uni-bayreuth.de

Authors

Ryushi Fujimura − *Graduate School of Regional Development and Creativity, Utsunomiya University, Utsunomiya 321-8585, Japan*

Markus Retsch − *Department of Chemistry, Physical Chemistry I, University of Bayreuth, Bayreuth 95447, Germany;* orcid.org/0000-0003-2629-8450

Complete contact information is available at: https://pubs.acs.org/10.1021/acs.jpcc.3c03307

Notes

The authors declare no competing financial interest.

■ ACKNOWLEDGMENTS

This project has received funding from the European Research Council (ERC) under the European Union's Horizon 2020 research and innovation program (grant agreement no. 714968).

■ REFERENCES

(1) Li, W.; Valentine, J. G. Harvesting the Loss: Surface Plasmon-Based Hot Electron Photodetection. *NANO* **2017**, *6*, 177−191.

(2) Liu, X.; Tyler, T.; Starr, T.; Starr, A. F.; Jokerst, N. M.; Padilla, W. J. Taming the Blackbody with Infrared Metamaterials as Selective Thermal Emitters. *Phys. Rev. Lett.* **2011**, *107*, No. 045901.

(3) Azad, A. K.; Kort-Kamp, W. J. M.; Sykora, M.; Weisse-Bernstein, N. R.; Luk, T. S.; Taylor, A. J.; Dalvit, D. A. R.; Chen, H.-T. Metasurface Broadband Solar Absorber. *Sci. Rep.* **2016**, *6*, 20347.

(4) Hossain, M.; Gu, M. Radiative Cooling: Principles, Progress, and Potentials. *Adv. Sci.* **2016**, *3*, 1500360.

(5) Liu, N.; Mesch, M.; Weiss, T.; Hentschel, M.; Giessen, H. Infrared Perfect Absorber and Its Application as Plasmonic Sensor. *Nano Lett.* **2010**, *10*, 2342−2348.

(6) Chen, K.; Adato, R.; Altug, H. Dual-Band Perfect Absorber for Multispectral Plasmon-Enhanced Infrared Spectroscopy. *ACS Nano* **2012**, *6*, 7998−8006.

(7) Takei, H.; Bessho, N.; Ishii, A.; Okamoto, T.; Beyer, A.; Vieker, H.; Gölzhäuser, A. Enhanced Infrared Lspr Sensitivity of Cap-Shaped Gold Nanoparticles Coupled to a Metallic Film. *Langmuir* **2014**, *30*, 2297−2305.

(8) Lee, N.; Kim, T.; Lim, J. S.; Chang, I.; Cho, H. H. Metamaterial-Selective Emitter for Maximizing Infrared Camouflage Performance with Energy Dissipation. *ACS Appl. Mater. Interfaces* **2019**, *11*, 21250−21257.

(9) Baffou, G.; Quidant, R.; Girard, C. Heat Generation in Plasmonic Nanostructures: Influence of Morphology. *Appl. Phys. Lett.* **2009**, *94*, No. 153109.

(10) Baffou, G.; Quidant, R.; García de Abajo, F. J. Nanoscale Control of Optical Heating in Complex Plasmonic Systems. *ACS Nano* **2010**, *4*, 709−716.

(11) Metwally, K.; Mensah, S.; Baffou, G. Isosbestic Thermoplasmonic Nanostructures. *ACS Photonics* **2017**, *4*, 1544−1551.

(12) Landy, N. I.; Sajuyigbe, S.; Mock, J. J.; Smith, D. R.; Padilla, W. J. Perfect Metamaterial Absorber. *Phys. Rev. Lett.* **2008**, *100*, No. 207402.

(13) Wu, C.; Neuner, B.; Shvets, G.; John, J.; Milder, A.; Zollars, B.; Savoy, S. Large-Area Wide-Angle Spectrally Selective Plasmonic Absorber. *Phys. Rev. B* **2011**, *84*, No. 075102.

(14) Hao, J.; Zhou, L.; Qiu, M. Nearly Total Absorption of Light and Heat Generation by Plasmonic Metamaterials. *Phys. Rev. B* **2011**, *83*, No. 165107.

(15) Tittl, A.; Harats, M. G.; Walter, R.; Yin, X.; Schäferling, M.; Liu, N.; Rapaport, R.; Giessen, H. Quantitative Angle-Resolved Small-Spot Reflectance Measurements on Plasmonic Perfect Absorbers: Impedance Matching and Disorder Effects. *ACS Nano* **2014**, *8*, 10885−10892.

(16) Kwon, D. H.; Pozar, D. M. Optimal Characteristics of an Arbitrary Receive Antenna. *IEEE Trans. Antennas Propag.* **2009**, *57*, 3720−3727.

(17) Ra'di, Y.; Asadchy, V. S.; Kosulnikov, S. U.; Omelyanovich, M. M.; Morits, D.; Osipov, A. V.; Simovski, C. R.; Tretyakov, S. A. Full Light Absorption in Single Arrays of Spherical Nanoparticles. *ACS Photonics* **2015**, *2*, 653−660.

(18) Dezert, R.; Richetti, P.; Baron, A. Complete Multipolar Description of Reflection and Transmission across a Metasurface for Perfect Absorption of Light. *Opt. Express* **2019**, *27*, 26317−26330.

(19) Jang, M. S.; Atwater, H. Plasmonic Rainbow Trapping Structures for Light Localization and Spectrum Splitting. *Phys. Rev. Lett.* **2011**, *107*, No. 207401.

(20) Cui, Y.; Fung, K. H.; Xu, J.; Ma, H.; Jin, Y.; He, S.; Fang, N. X. Ultrabroadband Light Absorption by a Sawtooth Anisotropic Metamaterial Slab. *Nano Lett.* **2012**, *12*, 1443−1447.

(21) Ji, D.; Song, H.; Zeng, X.; Hu, H.; Liu, K.; Zhang, N.; Gan, Q. Broadband Absorption Engineering of Hyperbolic Metafilm Patterns. *Sci. Rep.* **2014**, *4*, 4498.

(22) Akulshin, A. M.; Barreiro, S.; Lezama, A. Electromagnetically Induced Absorption and Transparency Due to Resonant Two-Field Excitation of Quasidegenerate Levels in Rb Vapor. *Phys. Rev. A* **1998**, *57*, 2996−3002.

(23) Lezama, A.; Barreiro, S.; Akulshin, A. M. Electromagnetically Induced Absorption. *Phys. Rev. A* **1999**, *59*, 4732−4735.

(24) Garrido Alzar, C. L.; Martinez, M. A. G.; Nussenzveig, P. Classical Analog of Electromagnetically Induced Transparency. *Am. J. Phys.* **2002**, *70*, 37−41.

(25) Taubert, R.; Hentschel, M.; Kästel, J.; Giessen, H. Classical Analog of Electromagnetically Induced Absorption in Plasmonics. *Nano Lett.* **2012**, *12*, 1367−1371.

(26) Taubert, R.; Hentschel, M.; Giessen, H. Plasmonic Analog of Electromagnetically Induced Absorption: Simulations, Experiments,

and Coupled Oscillator Analysis. *J. Opt. Soc. Am. B* **2013**, *30*, 3123−3134.
(27) Tassin, P.; Zhang, L.; Zhao, R.; Jain, A.; Koschny, T.; Soukoulis, C. M. Electromagnetically Induced Transparency and Absorption in Metamaterials: The Radiating Two-Oscillator Model and Its Experimental Confirmation. *Phys. Rev. Lett.* **2012**, *109*, No. 187401.
(28) Wan, M.-L.; He, J.-N.; Song, Y.-L.; Zhou, F.-Q. Electromagnetically Induced Transparency and Absorption in Plasmonic Metasurfaces Based on near-Field Coupling. *Phys. Lett. A* **2015**, *379*, 1791−1795.
(29) Zhang, F.; Huang, X.; Cai, W.; Yang, R.; Fu, Q.; Fan, Y.; Hu, Y.; Qiu, K.; Zhang, W.; Li, C.; Li, Q. Eia Metamaterials Based on Hybrid Metal/Dielectric Structures with Dark-Mode-Enhanced Absorption. *Opt. Express* **2020**, *28*, 17481−17489.
(30) He, J.; Ding, P.; Wang, J.; Fan, C.; Liang, E. Ultra-Narrow Band Perfect Absorbers Based on Plasmonic Analog of Electromagnetically Induced Absorption. *Opt. Express* **2015**, *23*, 6083−6091.
(31) Xiong, W.; Wang, W.; Ling, F.; Yu, W.; Yao, J. Modulation of Terahertz Electromagnetically Induced Absorption Analogue in a Hybrid Metamaterial/Graphene Structure. *AIP Adv.* **2019**, *9*, No. 115314.
(32) Zhang, T.; Dai, J.; Dai, Y.; Fan, Y.; Han, X.; Li, J.; Yin, F.; Zhou, Y.; Xu, K. Dynamically Tunable Plasmon Induced Absorption in Graphene-Assisted Metallodielectric Grating. *Opt. Express* **2017**, *25*, 26221−26233.
(33) Krauth, J.; Schumacher, T.; Defrance, J.; Metzger, B.; Lippitz, M.; Weiss, T.; Giessen, H.; Hentschel, M. Nonlinear Spectroscopy on the Plasmonic Analog of Electromagnetically Induced Absorption: Revealing Minute Structural Asymmetries. *ACS Photonics* **2019**, *6*, 2850−2859.
(34) Matsumori, K.; Fujimura, R.; Retsch, M. Coupling Strength and Total Damping Govern Electromagnetically Induced Absorption in Coupled Plasmonic Systems. *Adv. Photonics Res.* **2023**, *4*, 2200211.
(35) Fleury, R.; Soric, J.; Alù, A. Physical Bounds on Absorption and Scattering for Cloaked Sensors. *Phys. Rev. B* **2014**, *89*, No. 045122.
(36) Tretyakov, S. Maximizing Absorption and Scattering by Dipole Particles. *Plasmonics* **2014**, *9*, 935−944.
(37) Alaee, R.; Albooyeh, M.; Rockstuhl, C. Theory of Metasurface Based Perfect Absorbers. *J. Phys. D: Appl. Phys.* **2017**, *50*, No. 503002.
(38) Grigoriev, V.; Bonod, N.; Wenger, J.; Stout, B. Optimizing Nanoparticle Designs for Ideal Absorption of Light. *ACS Photonics* **2015**, *2*, 263−270.
(39) Prodan, E.; Nordlander, P. Plasmon Hybridization in Spherical Nanoparticles. *J. Chem. Phys.* **2004**, *120*, 5444−5454.
(40) Nordlander, P.; Prodan, E. Plasmon Hybridization in Nanoparticles near Metallic Surfaces. *Nano Lett.* **2004**, *4*, 2209−2213.
(41) Baur, S.; Sanders, S.; Manjavacas, A. Hybridization of Lattice Resonances. *ACS Nano* **2018**, *12*, 1618−1629.
(42) Liu, N.; Mukherjee, S.; Bao, K.; Brown, L. V.; Dorfmüller, J.; Nordlander, P.; Halas, N. J. Magnetic Plasmon Formation and Propagation in Artificial Aromatic Molecules. *Nano Lett.* **2012**, *12*, 364−369.
(43) Li, Z.; You, Q.; Wang, H.; Zhang, L.; Zhang, D.; Jia, S.; Fang, Y.; Wang, P. Nanowire Dimer Optical Antenna Brightens the Surface Defects of Silicon. *NANO* **2023**, *12*, 1723−1731.
(44) Kekatpure, R. D.; Barnard, E. S.; Cai, W.; Brongersma, M. L. Phase-Coupled Plasmon-Induced Transparency. *Phys. Rev. Lett.* **2010**, *104*, No. 243902.
(45) Lu, H.; Liu, X.; Mao, D.; Wang, G. Plasmonic Nanosensor Based on Fano Resonance in Waveguide-Coupled Resonators. *Opt. Lett.* **2012**, *37*, 3780−3782.
(46) Dahmen, C.; Schmidt, B.; von Plessen, G. Radiation Damping in Metal Nanoparticle Pairs. *Nano Lett.* **2007**, *7*, 318−322.
(47) Taubert, R.; Ameling, R.; Weiss, T.; Christ, A.; Giessen, H. From near-Field to Far-Field Coupling in the Third Dimension: Retarded Interaction of Particle Plasmons. *Nano Lett.* **2011**, *11*, 4421−4424.
(48) Tan, W.; Sun, Y.; Wang, Z.-G.; Chen, H. Manipulating Electromagnetic Responses of Metal Wires at the Deep Subwavelength Scale Via Both near- and Far-Field Couplings. *Appl. Phys. Lett.* **2014**, *104*, No. 091107.
(49) Zhong, J.; Huang, C. Crowding Effects of Nanoparticles on Energy Absorption in Solar Absorption Coatings. *J. Appl. Phys.* **2019**, *125*, No. 033103.
(50) Rolly, B.; Stout, B.; Bonod, N. Metallic Dimers: When Bonding Transverse Modes Shine Light. *Phys. Rev. B* **2011**, *84*, No. 125420.
(51) Ma, L. X.; Wang, C. C. Isosbestic Light Absorption by Metallic Dimers: Effect of Interparticle Electromagnetic Coupling. *Appl. Opt.* **2020**, *59*, 1028−1036.
(52) Hugonin, J.-P.; Besbes, M.; Ben-Abdallah, P. Fundamental Limits for Light Absorption and Scattering Induced by Cooperative Electromagnetic Interactions. *Phys. Rev. B* **2015**, *91*, No. 180202.
(53) Markovich, D.; Baryshnikova, K.; Shalin, A.; Samusev, A.; Krasnok, A.; Belov, P.; Ginzburg, P. Enhancement of Artificial Magnetism Via Resonant Bianisotropy. *Sci. Rep.* **2016**, *6*, 22546.
(54) Floess, D.; Hentschel, M.; Weiss, T.; Habermeier, H.-U.; Jiao, J.; Tikhodeev, S. G.; Giessen, H. Plasmonic Analog of Electromagnetically Induced Absorption Leads to Giant Thin Film Faraday Rotation of 14°. *Phys. Rev. X* **2017**, *7*, No. 021048.
(55) Jackson, J. D., *Classical Electrodynamics*; John Wiley & Sons: New York, 1962.
(56) Schlather, A. E.; Large, N.; Urban, A. S.; Nordlander, P.; Halas, N. J. Near-Field Mediated Plexcitonic Coupling and Giant Rabi Splitting in Individual Metallic Dimers. *Nano Lett.* **2013**, *13*, 3281−3286.
(57) Huang, Y.; Ma, L.; Hou, M.; Li, J.; Xie, Z.; Zhang, Z. Hybridized Plasmon Modes and near-Field Enhancement of Metallic Nanoparticle-Dimer on a Mirror. *Sci. Rep.* **2016**, *6*, 30011.
(58) Yang, Z. J.; Antosiewicz, T. J.; Shegai, T. Role of Material Loss and Mode Volume of Plasmonic Nanocavities for Strong Plasmon-Exciton Interactions. *Opt. Express* **2016**, *24*, 20373−20381.
(59) Albella, P.; Poyli, M. A.; Schmidt, M. K.; Maier, S. A.; Moreno, F.; Sáenz, J. J.; Aizpurua, J. Low-Loss Electric and Magnetic Field-Enhanced Spectroscopy with Subwavelength Silicon Dimers. *J. Phys. Chem. C* **2013**, *117*, 13573−13584.
(60) Sun, S.; Li, M.; Du, Q.; Png, C. E.; Bai, P. Metal−Dielectric Hybrid Dimer Nanoantenna: Coupling between Surface Plasmons and Dielectric Resonances for Fluorescence Enhancement. *J. Phys. Chem. C* **2017**, *121*, 12871−12884.
(61) Bakker, R. M.; Permyakov, D.; Yu, Y. F.; Markovich, D.; Paniagua-Domínguez, R.; Gonzaga, L.; Samusev, A.; Kivshar, Y.; Luk'yanchuk, B.; Kuznetsov, A. I. Magnetic and Electric Hotspots with Silicon Nanodimers. *Nano Lett.* **2015**, *15*, 2137−2142.
(62) Mulholland, G. W.; Bohren, C. F.; Fuller, K. A. Light Scattering by Agglomerates: Coupled Electric and Magnetic Dipole Method. *Langmuir* **1994**, *10*, 2533−2546.
(63) Merchiers, O.; Moreno, F.; González, F.; Saiz, J. M. Light Scattering by an Ensemble of Interacting Dipolar Particles with Both Electric and Magnetic Polarizabilities. *Phys. Rev. A* **2007**, *76*, No. 043834.
(64) Matsumori, K.; Fujimura, R.; Retsch, M. Selective Broadband Absorption by Mode Splitting for Radiative Cooling. *Opt. Express* **2022**, *30*, 14258−14273.
(65) Bohren, C. F.; Huffman, D. R., *Absorption and Scattering of Light by Small Particles*; John Wiley & Sons, 2008.
(66) Zhang, C.; Chen, B.-Q.; Li, Z.-Y.; Xia, Y.; Chen, Y.-G. Surface Plasmon Resonance in Bimetallic Core−Shell Nanoparticles. *J. Phys. Chem. C* **2015**, *119*, 16836−16845.
(67) van de Groep, J.; Polman, A. Designing Dielectric Resonators on Substrates: Combining Magnetic and Electric Resonances. *Opt. Express* **2013**, *21*, 26285−26302.
(68) Staude, I.; Schilling, J. Metamaterial-Inspired Silicon Nanophotonics. *Nat. Photonics* **2017**, *11*, 274−284.
(69) Shkondin, E.; Takayama, O.; Panah, M. E. A.; Liu, P.; Larsen, P. V.; Mar, M. D.; Jensen, F.; Lavrinenko, A. V. Large-Scale High

Aspect Ratio Al-Doped Zno Nanopillars Arrays as Anisotropic Metamaterials. *Opt. Mater. Express* **2017**, *7*, 1606−1627.
(70) Weiting, F.; Yixun, Y. Temperature Effects on the Refractive Index of Lead Telluride and Zinc Selenide. *Infrared Phys.* **1990**, *30*, 371−373.
(71) Krishnamoorthy, H. N. S.; Adamo, G.; Yin, J.; Savinov, V.; Zheludev, N. I.; Soci, C. Infrared Dielectric Metamaterials from High Refractive Index Chalcogenides. *Nat. Commun.* **2020**, *11*, 1692.
(72) Zhang, X.; Qiu, J.; Zhao, J.; Li, X.; Liu, L. Complex Refractive Indices Measurements of Polymers in Infrared Bands. *J. Quant. Spectrosc. Radiat. Transfer* **2020**, *252*, No. 107063.
(73) Evlyukhin, A. B.; Fischer, T.; Reinhardt, C.; Chichkov, B. N. Optical Theorem and Multipole Scattering of Light by Arbitrarily Shaped Nanoparticles. *Phys. Rev. B* **2016**, *94*, No. 205434.
(74) Paniagua-Domínguez, R.; Yu, Y. F.; Miroshnichenko, A. E.; Krivitsky, L. A.; Fu, Y. H.; Valuckas, V.; Gonzaga, L.; Toh, Y. T.; Kay, A. Y. S.; Luk'yanchuk, B.; Kuznetsov, A. I. Generalized Brewster Effect in Dielectric Metasurfaces. *Nat. Commun.* **2016**, *7*, 10362.
(75) Terekhov, P. D.; Baryshnikova, K. V.; Artemyev, Y. A.; Karabchevsky, A.; Shalin, A. S.; Evlyukhin, A. B. Multipolar Response of Nonspherical Silicon Nanoparticles in the Visible and near-Infrared Spectral Ranges. *Phys. Rev. B* **2017**, *96*, No. 035443.
(76) Alaee, R.; Rockstuhl, C.; Fernandez-Corbaton, I. An Electromagnetic Multipole Expansion Beyond the Long-Wavelength Approximation. *Opt. Commun.* **2018**, *407*, 17−21.
(77) Miroshnichenko, A. E.; Evlyukhin, A. B.; Yu, Y. F.; Bakker, R. M.; Chipouline, A.; Kuznetsov, A. I.; Luk'yanchuk, B.; Chichkov, B. N.; Kivshar, Y. S. Nonradiating Anapole Modes in Dielectric Nanoparticles. *Nat. Commun.* **2015**, *6*, 8069.
(78) Baryshnikova, K. V.; Smirnova, D. A.; Luk'yanchuk, B. S.; Kivshar, Y. S. Optical Anapoles: Concepts and Applications. *Adv. Opt. Mater.* **2019**, *7*, 1801350.
(79) Hüttenhofer, L.; Tittl, A.; Kühner, L.; Cortés, E.; Maier, S. A. Anapole-Assisted Absorption Engineering in Arrays of Coupled Amorphous Gallium Phosphide Nanodisks. *ACS Photonics* **2021**, *8*, 1469−1476.
(80) Li, Z.; You, Q.; Li, J.; Zhu, C.; Zhang, L.; Yang, L.; Fang, Y.; Wang, P. Boosting Light−Matter Interaction in a Longitudinal Bonding Dipole Plasmon Hybrid Anapole System. *J. Phys. Chem. C* **2023**, *127*, 3594−3601.
(81) Evlyukhin, A. B.; Reinhardt, C.; Zywietz, U.; Chichkov, B. N. Collective Resonances in Metal Nanoparticle Arrays with Dipole-Quadrupole Interactions. *Phys. Rev. B* **2012**, *85*, No. 245411.
(82) Kats, M. A.; Yu, N.; Genevet, P.; Gaburro, Z.; Capasso, F. Effect of Radiation Damping on the Spectral Response of Plasmonic Components. *Opt. Express* **2011**, *19*, 21748−21753.
(83) Zuloaga, J.; Nordlander, P. On the Energy Shift between near-Field and Far-Field Peak Intensities in Localized Plasmon Systems. *Nano Lett.* **2011**, *11*, 1280−1283.
(84) Alonso-González, P.; Albella, P.; Neubrech, F.; Huck, C.; Chen, J.; Golmar, F.; Casanova, F.; Hueso, L. E.; Pucci, A.; Aizpurua, J.; Hillenbrand, R. Experimental Verification of the Spectral Shift between near- and Far-Field Peak Intensities of Plasmonic Infrared Nanoantennas. *Phys. Rev. Lett.* **2013**, *110*, No. 203902.
(85) Januar, M.; Liu, B.; Cheng, J. C.; Hatanaka, K.; Misawa, H.; Hsiao, H. H.; Liu, K. C. Role of Depolarization Factors in the Evolution of a Dipolar Plasmonic Spectral Line in the Far- and near-Field Regimes. *J. Phys. Chem. C* **2020**, *124*, 3250−3259.

https://doi.org/10.1021/acs.jpcc.3c03307
J. Phys. Chem. C 2023, 127, 19127−19140